Multivariate empirical mode decomposition approach for adaptive denoising of fringe patterns

Xiang Zhou,* Tao Yang, Haihua Zou, and Hong Zhao

State Key Laboratory for Manufacturing Systems Engineering, Xi'an Jiaotong University, Xi'an, Shaanxi, 710049, China
**Corresponding author: zhouxiang@xjtu.edu.cn*

Received February 14, 2012; revised March 27, 2012; accepted April 10, 2012;
posted April 10, 2012 (Doc. ID 163083); published May 23, 2012

An adaptive approach is presented for noise reduction of optical fringe patterns using multivariate empirical mode decomposition. Adjacent rows and columns of patterns are treated as multichannel signals and are decomposed into multiscale components. Fringe patterns are reconstructed with less noise by simply thresholding coefficients in different scales. The proposed approach can better concentrate local main components of fringe signals into single scale, compared with the conventional multiscale denoising method. A simulated pattern and an actual example are examined. Signal-to-noise ratio (SNR) of the simulated pattern is more than doubled. © 2012 Optical Society of America

OCIS codes: 100.2650, 120.2650.

The empirical mode decomposition (EMD) algorithm has become an established tool for time-frequency analysis of nonstationary signals in recent years [1]. EMD and its variants are also currently used to analyze fringe patterns for denoising, detrending, and phase retrieval. Bernini *et al.* used the standard EMD to reduce noise and normalize fringes in a digital speckle pattern [2]. Li *et al.* utilized one dimensional (1D) EMD to eliminate zero spectrum in the Fourier transform profilometry [3]. Moreover, bidimensional EMD (BEMD) has been applied to analyze speckle patterns [4] and amplitude-encoded fringe patterns [5]. BEMD overcomes the problem of 1D implementation that ignores the correlation among rows or columns of an image and leads to unsatisfactory results for some fringes such as closed fringes [4].

EMD-based methods still have inherent limits in handling fringe patterns despite their good adaptability and locality [6]. A frustrating problem with both EMD and BEMD is the mode mixing caused by intermittent noise in different scales of data. Noise in a fringe pattern, in many situations, is discontinuously distributed or submerged in the fringes with large amplitudes such that separating the noise and the fringes is quite challenging. We used a 1D ensemble EMD (EEMD) [6] for carrier fringe analysis to alleviate this problem. Bernini *et al.* [7] and Zhou *et al.* [8] used bidimensional EEMD for speckle patterns. However, the implementation of EEMD requires the interpolation of curves or surfaces hundreds of times and is, therefore, extremely time-consuming.

We present in this letter a novel and adaptive method to denoise fringe patterns using multivariate EMD (MEMD), a newly developed signal-processing tool [9]. MEMD extends the original EMD to multichannel signals and works as adaptive filter banks with scale alignment of channels. The adjacent rows and columns of fringe patterns, which are treated as multichannel signals, are decomposed into multiscale components in the proposed method. Fringe patterns are reconstructed with less noise by simply thresholding coefficients in different scales. The proposed method, compared with conventional multiscale methods such as wavelets, windowed Fourier transform, and other EMD-based approaches, can better concentrate local main components of a fringe signal into one scale while driving noises to other scales. A simulated pattern, as well as an actual example, are examined using the proposed method.

A typical implementation of MEMD proposed in [9] generates multiple n-dimensional envelopes by taking signal projections along different directions in n-dimensional spaces. These projections are then averaged to obtain the local mean. The direction vectors for taking projections are chosen to be based on a low-discrepancy Hammersley sequence that generates a more uniform pointset than a spherical coordinate system. The remainder of the procedure is quite similar to the standard EMD summarized in [1] once the mean signal is defined. More specifically, a sequence of N-dimensional vectors $\{\mathbf{v}(x)\}_{t=1}^{T} = \{v_1(x), v_2(x), \ldots, v_N(x)\}$ represents a multivariate signal with N components, and $\mathbf{h}^{\theta_k} = \{h_1^k, h_2^k, \ldots, h_N^k\}$ denotes a set of direction vectors along the directions given by angles $\theta^k = \{\theta_1^k, \theta_2^k, \ldots, \theta_{(N-1)}^k\}$ on an $(N-1)$ sphere. The proposed multivariate extension of EMD, suitable for general nonlinear and nonstationary n-variate time series operations, is summarized in the algorithm below:

1. Choose a suitable pointset for sampling on an $(N-1)$-sphere based on a low-discrepancy Hammersley sequence.
2. Calculate a projection, denoted by $p^{\theta_k}(t)$, of the input signal $\mathbf{v}(x)$ along the direction vector $\mathbf{h}^{\theta_k}$, for all k (the whole set of direction vectors), giving $\{p^{\theta_k}(x)\}_{k=1}^{K}$ as the set of projections.
3. Find the time instants $\{x_i^{\theta_k}\}$ corresponding to the maxima of the set of projected signals $\{p^{\theta_k}(x)\}_{k=1}^{K}$.
4. Interpolate $[x_i^{\theta_k}, \mathbf{v}(x_i^{\theta_k})]$ to obtain multivariate envelope curves $\{\mathbf{e}^{\theta_k}(x)\}_{k=1}^{K}$.
5. For a set of K direction vectors, the mean $\mathbf{m}(\mathrm{x})$ of the envelope curves is calculated as $\mathbf{m}(x) = K^{-1}\sum_{k=1}^{K} \mathbf{e}^{\theta_k}(x)$.
6. Extract the "detail" $\mathbf{d}(x)$ using $\mathbf{d}(x) = \mathbf{v}(x) - \mathbf{m}(x)$. If the "detail" $\mathbf{d}(x)$ fulfills the stoppage criterion for a multivariate intrinsic mode function (IMF), then apply the above procedure to $\mathbf{v}(x) - \mathbf{d}(x)$, otherwise apply it to $\mathbf{d}(x)$.

0146-9592/12/111904-03$15.00/0

The following 2D fringe pattern is considered:

$$I(x,y) = a(x,y) + b(x,y)\cos\phi(x,y) + n(x,y), \quad (1)$$

where $I(x,y)$, $a(x,y)$, and $b(x,y)$ are the recorded intensity, background intensity, and fringe amplitude, respectively. $\phi(x,y)$ is the phase distribution, and $n(x,y)$ is the randomly distributed noise. We denote $u_i(x)$ as the ith row of $I(x,y)$ for a digital fringe pattern of $M \times N$ pixels. Then, $\mathbf{u}(x) = \{u_{i-L}(x), u_{i-L+1}(x), \ldots, u_{i+L}(x)\}$ represents a multivariate signal with $2L+1$ components, namely, $2L+1$ rows of the fringe pattern with L as a number between 1 and 7. Taking $\mathbf{u}(x)$ as the input signal of the MEMD algorithm above, we find a set of P multivariate IMFs $\{\mathbf{c}^j(x)\}_{j=1}^P$ and a multivariate residue $\mathbf{r}(x)$ so that

$$\mathbf{u}(x) = \sum_{j=1}^{P} \mathbf{c}^j(x) + \mathbf{r}(x), \quad (2)$$

where $\mathbf{c}^j(x)$ and $\mathbf{r}(x)$ contain $2L+1$ univariate IMFs $\{c_{i-L}^j(x), c_{i-L+1}^j(x), \ldots, c_{i+L}^j(x)\}$ and $2L+1$ univariate residues $\{r_{i-L}(x), r_{i-L+1}(x), \ldots, r_{i+L}(x)\}$, respectively. The component $u_i(x)$ can also be written as a sum of a group of univariate IMFs at all levels and a univariate residue $u_i(x) = \sum_{j=1}^{P} c_i^j(x) + r_i(x)$ which is different from the standard EMD. The difference is exhibited in the following aspects: (1) No mode-mixing. Even a weak noise in multivariate signals can constitute a complete IMF by a MEMD operation. The reason is that small and fast fluctuations hidden in the large and the slow signals, which could not be extracted by standard EMD, can be detected by projecting multivariate signals along various directions of a sphere; and (2) locally adaptive filtering, which means that local noises and main components of a signal, such as modulated parts, are adaptively allocated to different IMFs. In particular, main components in any local position will concentrate in no more than one IMF while the whole of them may be distributed in several adjacent IMFs, provided that the spectrum of the signal in a local area is simpler than the spectra of the signals in the whole field. This condition is different from wavelet and EEMD, which usually act as fixed filter banks in the whole space domain and possibly divide the main component of a local position into two neighboring scales [10]. Benefiting from these two points, SNR at every scale is expected to be high, which allows us to easily reduce the noise from fringe signals by merely eliminating coefficients of IMFs with small amplitude as similarly done in discrete wavelet transform (DWT).

A simulated carrier fringe pattern shown in Fig. 1(a) is contaminated by heavy speckle noise and is used to

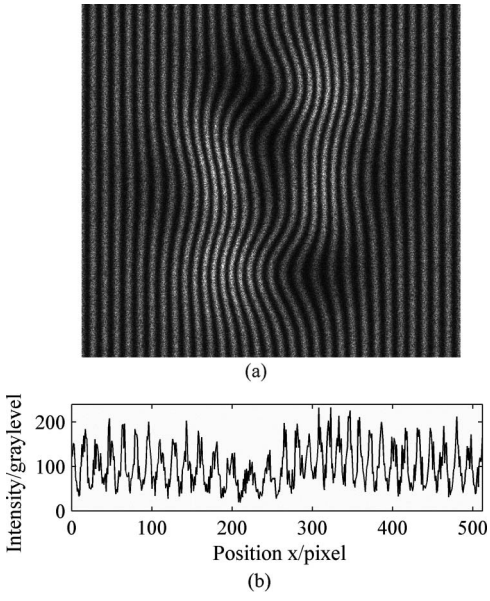

Fig. 1. (a) Simulated noisy fringe pattern and (b) its 115th row signal.

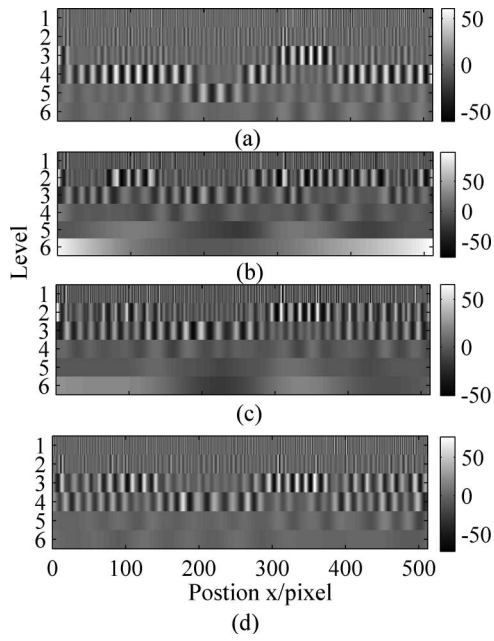

Fig. 2. IMFs (levels 1 to 6) generated from (a) MEMD, (b) EMD, and (c) EEMD. (d) DWT details decomposed by a db9 wavelet.

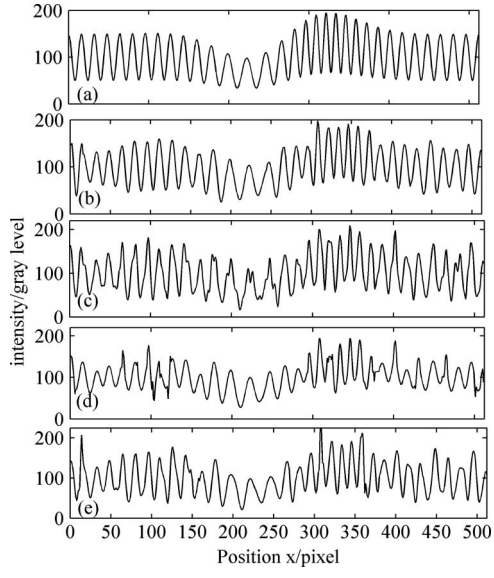

Fig. 3. Denoised results of the 115th row: (a) the ideal signal and the signals denoised by (b) MEMD, (c) EMD, (d) EEMD, and (e) DWT.

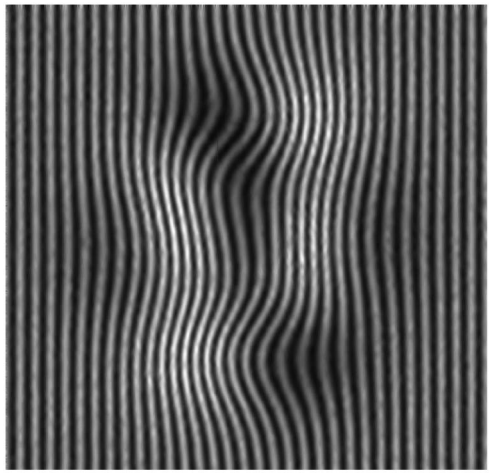

Fig. 4. Denoised fringe pattern handled first along rows and then along columns.

verify the proposed method. The SNR of the pattern is 12.8 dB, and the image size is 512×512 pixels. The 115th row signal, demonstrating the noise, is illustrated in Fig. 1(b). The phase distribution is modulated by the peak function provided by the Matlab function. Background intensity is simulated to be proportional to the first phase derivative.

We apply the algorithm to each row of the pattern with $L = 2$. For example, Fig. 2(a) presents the results of the decomposition of MEMD on the 115th row, including six IMFs from levels 1 to 6. The results from the standard EMD, EEMD, and db9-based DWT are also given in Figs. 2(b), 2(c), and 2(d), respectively. All decompositions clearly work as filter banks that filter the signal to a decreasing frequency order. However, the MEMD approach concentrates much better the carrier components at local positions in a single band, unlike other approaches, facilitating the identified denoising process.

Our denoising strategy starts with the calculation of envelopes with the absolute value of the coefficients at different levels. Second, coefficients with local envelopes smaller than the threshold are set to zero, in contrast to common operations like DWT, to prevent the distortion of the carrier component. The threshold value in all levels is simply determined as half the maximum amplitude of the fringe pattern.

The ideal signal and the MEMD-denoised result are displayed in Figs. 3(a) and 3(b), respectively. The noise is not only greatly reduced, but the recovered signal is also shown to be very close to the ideal signal. The results from the standard EMD, EEMD, and DWT are also presented for comparison in Figs. 3(c), 3(d), and 3(e), respectively. Some noise evidently remains, and a large distortion to the ideal signal occurs because SNRs at levels 2 to 4 are too low for the thresholding to eliminate majority of the noise. In the latter three methods, a level-dependent threshold $\lambda_P = \sqrt{2 \ln N}\sigma_P$ is employed for better performance, where N is the signal length, and σ_P is the noise level estimated by the median absolute deviation of the coefficients at level P.

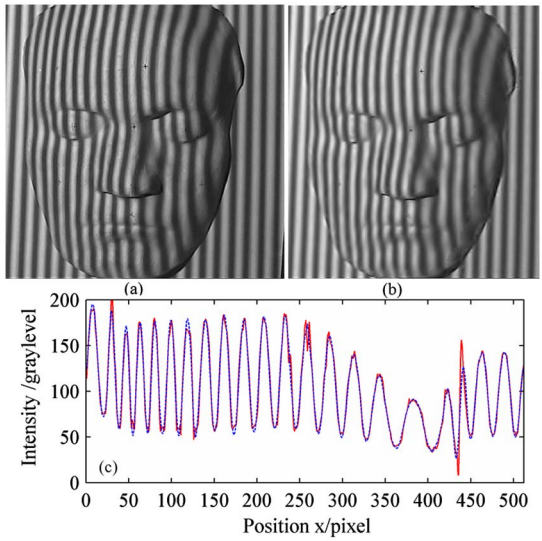

Fig. 5. (Color online) (a) A real fringe-projected pattern and (b) the denoised result. (c) The 115th row before (solid line) and after (dotted line) denoising.

After denoising the pattern along rows, we continue to apply the same approach to the columns for two-dimensional denoising, which in total took nearly 2 min on a 2.66 GHz-CPU PC. The results are shown in Fig. 4. SNR increases to 28.5 dB, more than doubled, whereas 18.1, 19.6, and 21.5 dB SNRs are obtained for the standard EMD, EEMD, and DWT, respectively.

A real fringe-projected pattern on a plaster model, exhibited in Fig. 5(a), is examined, and the results are presented in Figs. 5(b) and 5(c). The noise is found to be well-suppressed, whereas carrier components and transient changes such as those around the face and the eyes are reserved to the highest degree.

This work was supported by the National Natural Science Foundation of China (51105301), the National Basic Research Program (2011CB706805), the Xian Scientific Research Plan (CXY1007), and the Innovation Fund for Undergraduate Research Training and Practice.

References

1. N. E. Huang, Z. Shen, S. R. Long, M. L. C. Wu, H. H. Shih, Q. N. Zheng, N. C. Yen, C. C. Tung, and H. H. Liu, P. Roy. Soc. Lond. A Mat. **454**, 903 (1998).
2. M. B. Bernini, G. E. Galizzi, A. Federico, and G. H. Kaufmann, Opt. Laser. Eng. **45**, 723 (2007).
3. S. Li, X. Su, W. Chen, and L. Xiang, J. Opt. Soc. Am. A **26**, 1195 (2009).
4. M. B. Bernini, A. Federico, and G. H. Kaufmann, Appl. Opt. **47**, 2592 (2008).
5. M. Wielgus and K. Patorski, Appl. Opt. **50**, 5513 (2011).
6. X. Zhou, H. Zhao, and T. Jiang, Opt. Lett. **34**, 2033 (2009).
7. M. B. Bernini, A. Federico, and G. H. Kaufmann, Appl. Opt. **50**, 641 (2011).
8. Y. Zhou and H. G. Li, Opt. Express **19**, 18207 (2011).
9. N. Rehman and D. P. Mandic, Soc. Lond. A Mat. **466**, 1291 (2010).
10. Z. Wu and N. E. Huang, Adv. Adapt. Data Anal. **1**, 1 (2009).